HHS Public Access

Author manuscript

J Am Chem Soc. Author manuscript; available in PMC 2020 March 20.

Published in final edited form as:

J Am Chem Soc. 2019 March 20; 141(11): 4764–4774. doi:10.1021/jacs.9b00558.

Thermally and Magnetically Robust Triplet Ground State Diradical.

Nolan Gallagher[†], **Hui Zhang**[†], **Tobias Junghoefer**[§], **Erika Giangrisostomi**[⊥], **Ruslan Ovsyannikov**[⊥], **Maren Pink**[‡], **Suchada Rajca**[†], **Maria Benedetta Casu**[*,§], and **Andrzej Rajca**[*,†]

[†]Department of Chemistry, University of Nebraska, Lincoln, Nebraska 68588-0304, USA.

[§]Institute of Physical and Theoretical Chemistry, University of Tübingen, 72076 Tübingen, Germany

[‡]Department of Chemistry, Indiana University, Bloomington, Indiana 47405-7102, USA.

[⊥]Helmholtz-Zentrum Berlin für Materialien und Energie (HZB), Albert-Einstein-Str 15, 12489 Berlin, Germany

Abstract

High spin ($S = 1$) organic diradicals may offer enhanced properties with respect to several emerging technologies, but typically exhibit low singlet triplet energy gaps and possess limited thermal stability. We report triplet ground state diradical **2** with a large singlet-triplet energy gap, $\Delta E_{ST} \geq 1.7$ kcal mol^{-1}, leading to nearly exclusive population of triplet ground state at room temperature, and good thermal stability with onset of decomposition at ~160 °C under inert atmosphere. Magnetic properties of **2** and the previously prepared diradical **1** are characterized by SQUID magnetometry of polycrystalline powders, in polystyrene glass, and in other matrices. Polycrystalline diradical **2** forms a novel one-dimensional (1D) spin-1 ($S = 1$) chain of organic radicals with intrachain antiferromagnetic coupling of $J'/k = -14$ K, which is associated with the N···N and N···O intermolecular contacts. The intrachain antiferromagnetic coupling in **2** is by far strongest among all studied 1D $S = 1$ chains of organic radicals, which also makes 1D $S = 1$ chains of **2** most isotropic, and therefore an excellent system for studies of low-dimensional magnetism. In polystyrene glass and in frozen benzene or dibutyl phthalate solution, both **1** and **2** are monomeric. Diradical **2** is thermally robust and is evaporated under ultra-high vacuum to form thin films of intact diradicals on silicon substrate, as demonstrated by X-ray photoelectron spectroscopy. Based on C-K NEXAFS spectra and AFM images of the ~1.5-nm thick films, the diradical molecules form islands on the substrate with molecules stacked approximately along the crystallographic *a*-axis. The films are stable under ultra-high vacuum for at least 60 h but show signs of decomposition when exposed to ambient conditions for 7 h.

[*]Corresponding Author: arajca1@unl.edu, benedetta.casu@uni-tuebingen.de.

ASSOCIATED CONTENT

Supporting Information

General procedures and materials, additional experimental details, X-ray crystallographic files for **2** in CIF format, stoichiometry and integrated XPS experimental signal intensities for the thin films of radical, fit results for the energy positions and relative intensities of the photoemission lines in the C 1s and N 1s spectra. This material is available free of charge via the Internet at http://pubs.acs.org.

The authors declare no competing financial interests.

Graphical Abstract

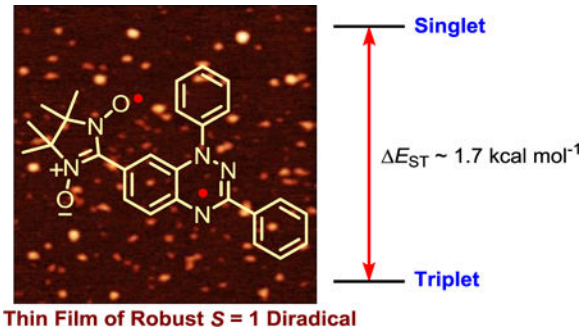

INTRODUCTION

Open-shell organic molecules with high-spin ground states and large energy gaps between the high-spin ground state and low-spin excited states possess unique, intriguing characteristics that are not only of fundamental interest but also have significant potential for numerous advanced technological applications. Notably, these molecules have long been considered the holy grail of purely organic magnets,[1–5] and recently have emerged as promising building blocks for organic spintronics,[6] spin filters,[7] sensors,[8] memory devices,[9] and probing quantum interference effects in molecular conductance.[10] Although the design principle has been well laid out,[11,12] such high-spin molecules with strong ferromagnetic interactions between unpaired electrons and persistence at room temperature remain highly uncommon,[13–16] and triplet ground state diradicals with robust thermal stabilities are especially rare.[17–19] The advancement in the design and synthesis of these exotic molecules will be crucial to the development of advanced organic magnetic materials and devices.

Recently, we reported triplet ground state diradicals with robust thermal stabilities, such as tetraazacyclophane diradical dication (TDD) and diradical **1** (Figure 1).[17,18] To our knowledge, these are the only two such diradicals that are well characterized with respect to stability by thermogravimetric analysis (TGA). Both TDD and **1** start decomposing at approximately 180 °C under nitrogen atmosphere and neutral diradical **1** could be sublimed under high vacuum at 140 °C without decomposition.

While these high-spin diradicals possess remarkable thermal properties, they are not fully populated in the high-spin state at room temperature. The singlet triplet energy gap, ΔE_{ST}, of both diradicals is only about 0.5 kcal mol^{-1}, as determined by quantitative EPR spectroscopy and SQUID magnetometry, which is similar to thermal energy at room temperature ($RT \approx 0.6$ kcal mol^{-1}).[17,18] In such a case, there is a significant depopulation of the triplet ground state at room temperature and above, and thus the unique magnetic properties of the high-spin state with extra-large magnetic moment are compromised at ambient temperatures.

To rectify this deficiency, we designed diradical **2** and preliminary computed its magnetic properties. The DFT calculations suggested an increased ΔE_{ST} by a factor of ~2.5, compared to **1**, and an estimated ~95+% occupancy of the triplet ground state at room temperature.[17]

We anticipated diradical **2** to possess both superior magnetic and excellent thermal properties, providing a novel high-spin diradical with robust high temperature stability and near-full occupation of the triplet ground state at ambient temperatures.

The potential of organic radicals in the development of organic electronics hinges upon their processability. The capacity of a molecule to form contacts or to evaporate onto a substrate without degradation is a critical prerequisite for device fabrication. In this regard, it is important to test the robustness of diradical **2** toward evaporation. Controlled evaporation of a diradical is considered very challenging, and to our knowledge, it has not been reported in literature. Achieving the first thin film of a high-spin diradical with nearly full-occupation of the triplet ground state at ambient temperature would be a significant step forward, providing exciting new avenues for the development of organic electronics.

Here we report the synthesis and study of high spin diradical **2** (Figure 1). As predicted, **2** has a large ΔE_{ST} of ≥1.7 kcal mol^{-1}, much larger than the thermal energy at room temperature, thus possessing a triplet ground state that is nearly exclusively populated (98+ %) at room temperature. For comparison, we characterize both **1** and **2** by SQUID magnetometry in dilute matrices and as polycrystalline powders. Notably, polycrystalline diradical **2** forms a novel one-dimensional (1D) spin-1 ($S = 1$) chain consisting of close contacts between the heteroatoms (oxygens and nitrogens) of radical moieties with the largest spin densities. The 1D chain is distinctly different from those previously reported,[18,20] and it is the first observed 1D system consisting of nitronyl nitroxide and Blatter radicals. Importantly, the observed intra-chain exchange coupling constant of $J'/k = -14$ K is much larger than the previously studied 1D $S = 1$ chains, with the next strongest $J'/k = -5.4$ K found in TDD.[18]Diradical **2** is thermally robust, with an onset of decomposition at ~160 °C under inert atmosphere and is thermally evaporated under ultra-high vacuum to form thin films on SiO_2/Si(111) wafers, with X-ray photoelectron spectroscopy suggesting the presence of intact **2**. The C-K NEXAFS spectra and AFM images of the films indicates the diradical molecules form islands on the substrate with molecules stacked approximately along the crystallographic *a*-axis. Diradical **2** possesses an unprecedented combination of a triplet ground state that is nearly exclusively populated at room temperature and a novel 1D $S = 1$ antiferromagnetic chain, with remarkable thermal stability and suitability for thin film deposition via thermal evaporation. The films are stable under ultra-high vacuum for at least 60 h but show signs of decomposition when exposed to ambient conditions for 7 h. We present here the preparation and characterization of the first thin film of high spin organic diradical.

RESULTS AND DISCUSSION

Synthesis of 2.

Our synthetic approach to **2**, follows closely the synthesis of diradical **1** and it takes advantage of the unusual stability of the Blatter radical, such that it may tolerate many common reaction conditions (Scheme 1).[21] Cyano-Blatter radical **3** is synthesized by adopting procedures available in the literature, as outlined in detail in the Supporting Information.[17,22–25] Treatment of **3** with DIBAL-H followed by hydrolysis of the imine

group provides formyl-Blatter radical **4**. Radical **4** is initially reduced to the corresponding *leuco*-amine-aldehyde, or alternatively, it is directly condensed with 2,3-bis(hydroxyamino)-2,3-dimethylbutane;[26] the resultant adduct is oxidized in air to provide diradical **2**, which is purified by normal phase chromatography (silica gel) at ambient conditions.

X-ray crystallography.

The structure of diradical **2** consists of two non-equivalent molecules, A and B, and one molecule of solvent (CH_2Cl_2). In molecule A, the nitronyl nitroxide radical moiety is nearly co-planar with the Blatter radical π-system with the corresponding N-C8A-C1A-C torsions in the –13 – (–15)° range, while in molecule B, there is considerably greater out-of-plane twisting with the corresponding torsions in the 28 – 30° range (Fig. S1, SI). In the crystal, molecules A and B pack in an alternating fashion into one-dimensional chains (along the crystallographic *a*-axis) with close intermolecular N···N and O···N contacts (Figure 2, bottom plot).

Within the π-conjugated pathway in the diradical, there are two dihedral angles of ~ 49° and 30° connecting the 1,2,4-benzotriazinyl and nitronyl nitroxide moieties in **1**,[17] as opposed to one dihedral angle (or one torsion) in **2**. The radicals in **2** are then more coplanar than in **1**. The DFT geometry optimizations using UB3LYP/6–31G(d) level of theory[27] and starting from either conformation as observed in molecule A or B give more co-planar structures that are similar to molecule A, with N-C8-C1-C torsions in the ±13.7 – (±13.8)° ranges (SI, Table S6).

EPR spectroscopy.

The EPR spectrum of **2** in glassy matrices shows exclusively a triplet diradical, without a trace of monoradical impurities (Figure 3, Table 1). As expected, the spectral simulation[28] reveals much greater spectral width, $2|D/hc| = 1.616 \times 10^{-2}$ for **2** vs. $2|D/hc| = 4.64 \times 10^{-3}$ for **1**,[17] because of relative proximity of the unpaired electrons and the nearly co-planar nitronyl nitroxide and benzotriazinyl moieties in **2**. The B3LYP/EPR-II calculations estimate the relative values of D as $D/hc = +1.20 \times 10^{-2}$ cm^{-1} for **2** and $D/hc = -5.47 \times 10^{-3}$ cm^{-1} for **1**.[29] The computed D-tensor components are not only overestimated, as typical for these type of diradicals, but also the positive sign of D/hc in **2** is inconsistent with its experimental EPR spectrum (Supporting Information).[30,31]

SQUID magnetometry: triplet ground states of 1 and 2.

We estimate singlet triplet energy gaps in polycrystalline **1** and **2** by fitting the χT vs. T data in the T = 1.8 – 320 K and 70 – 320 K ranges, respectively, to the diradical model (eq. 1).[4a]

$$\chi T = (1.118T/H)N\{2\sinh(a)/[1 + 2\cosh(a) + \exp((-2J/k)/T)]\} \quad (1)$$

$$a = 1.345(H/(T-\theta))$$

For **1**, an average of three fits (Figure 4 and SI, Fig. S8) gives $2J/k$ = 252 ± 10 K, corresponding to ΔE_{ST} = 0.50 ± 0.02 kcal mol^{-1} (Table 1), which is in good agreement with $2J/k$ = 234 ± 36 K, obtained previously by quantitative EPR spectroscopy in dilute solutions/matrices.[17] For **2**, a much larger $2J/k$ = 876 ± 36 K is obtained as an average of four fits (Figure 5 and SI: Fig. S9 and Table S2), corresponding to ΔE_{ST} = 1.74 ± 0.07 kcal mol^{-1} (Table 1). Although the measured values of χT > 0.75 emu K mol^{-1} and fitted values of ΔE_{ST} > 0 would suggest triplet ground states for **1** and **2**, these results are dependent on an accurate weight of the SQUID sample. Also, the fitting of χT vs. T for polycrystalline **1** and **2** require relatively large absolute values of negative mean-field parameters, $\theta \approx$ –6 and –14 K, thus suggesting significant antiferromagnetic interactions between the S = 1 diradicals.

With such large values of $|\theta|$, magnetization data at low temperatures could not be fit adequately to Brillouin functions, thus sample-weight independent evidence for triplet ground state could not be obtained. Therefore, we prepare dilute diradicals in glassy matrices by dispersing **1** and **2** in polystyrene.

For the dilute sample of **1** and **2** in polystyrene, two-parameter fits to χT vs. T data in the T = 1.8 – 370 and 1.8 – 360 K ranges give somewhat lower values of $2J/k$ = 165 ± 18 K and $2J/k$ = 838 ± 78 K (vs. polycrystalline diradicals), as an average of two and three fits, respectively (Figure 6 and SI: Figs. S11 and S12). Most importantly, these fits indicate that the value of θ is very small and practically negligible.

The magnetization (M) versus magnetic field (H) data, that is M versus $H/(T - \theta)$, at low temperatures (T = 1.8 – 5 K) provide excellent fits to the Brillouin functions with a small negative mean-field parameter, $|\theta| \leq$ 0.05 K. Such fits have two variable parameters: total spin (S) and magnetization at saturation (M_{sat}); the mean-field parameter θ is adjusted until the M/M_{sat} versus $H/(T - \theta)$ plots overlap at all temperatures. The values of $S \approx$ 1.0 (0.978−1.012), determined from the curvature of the Brillouin plots, unequivocally indicate the triplet (S = 1) ground state for both diradicals (Figure 6 and SI: Figs. S11 and S12). Since the values of M_{sat} = 0.74 and 0.925 μ_B for **1** and **2**, respectively (μ_B = Bohr magneton) match well the corresponding values of N = 0.73 and 0.93 obtained from fits of χT vs. T data to the diradical model, this implies that both diradicals are pure and N < 1.00 is obtained because of a “weighing error” of sub-milligram amounts of diradicals. The values of θ < 0 K and $|\theta| \approx$ 0 K imply nearly negligible, and almost certainly intermolecular, antiferromagnetic coupling.

We also investigate dilute diradicals in benzene and dibutylphthalate (DBP) matrices. Similar results are obtained for **1** and **2** in benzene and **2** in DBP; however, the fits to the Brillouin functions are less satisfactory because of much larger $|\theta|$ = 0.6 – 0.8 K observed in these matrices (SI, Table S3, Figs. S13 – S15).

SQUID magnetometry: 1D antiferromagnetic S = 1 chain for polycrystalline diradical 2.

For polycrystalline **1**, the χ vs. T plot shows continuously increasing χ with decreasing T. For **2**, a broad maximum at about 19 K in χ vs. T data is observed, thus suggesting relatively strong intermolecular coupling between S =1 diradicals **2** (Figures 4 and 5). Two limiting models for such antiferromagnetic coupling are considered: (1) one-dimensional (1-D)

Heisenberg chains of $S = 1$ diradicals (spin-1 chain) (eq. 2) and (2) pairs of $S = 1$ diradicals (dimer) (eq. S2, SI).[32,33] The numerical fits to these models are obtained at low temperatures, $T = 1.8$–70 K, to ensure that diradical **2** is almost completely in its $S = 1$ ground state at the highest temperature (70 K), which is significantly below $2J/k \approx 880$ K.

Initially, we fit χT vs. T data in the low temperature range, $T = 1.8 – 70$ K, using Eq. 2 and Eq. S2B (Table 2, Figure 5). 3-Parameter fits with the following variable parameters, intermolecular Heisenberg exchange coupling constant, J'/k, weight factor, N, and weight factor for isolated $S = 1$ diradical, N_{imp}, are in excellent agreement with 1D-chain model (coefficient of determination, $R^2 = 0.9999$ and standard error of estimate, $SEE = 0.0028$ or 0.0032); fits to an $S = 1$ dimer model are less satisfactory ($R^2 = 0.9998$ or 0.9994 and $SEE =$ 0.0043 or 0.0067). Even larger differences in fit quality between the two models are observed when the variable parameter N_{imp} is replaced with the mean-field parameter $\theta > 0$ (Table 2).

The χ versus T data provide a more sensitive measure of fit quality for different models. The fits to a 1D-chain (eq. 2) provide $SEE = 0.0002 – 0.0003$, while the $S = 1$ dimer fits (SI, eq. S2A) are much less satisfactory, with much larger $SEE = 0.0017 – 0.0089$, (Table 2, Figure 5).

$$\chi_{1D} = N\left\{[3/(2k(T-\theta))]\left[(2 + a_1 \times K + a_2 \times K^2)/(3 + b_1 \times K + b_2 \times K^2 + b_3 \times K^3)\right]\right\} \quad (2)$$
$$+ N_{imp}(1.118/H)\{2\sinh(a)/[1 + 2\cosh(a)]\}$$

$a_1 = 0.0194$, $a_2 = 0.777$, $b_1 = 4.346$, $b_2 = 3.232$, $b_3 = 5.634$,

$K = -J'/kT$ and $a = 1.345(H/(T - \theta))$

The 1D antiferromagnetic chain of weakly coupled $S = 1$ diradicals in polycrystalline **2** is consistent with the crystal packing, as discussed above (Figure 2). Two types of short N2A···N3B = 3.509 Å (dimer I) and O4B···N1A = 3.335 (dimer II) contacts between molecules A and B are identified. Because all nitrogens and oxygens in diradical **2** bear large positive spin densities, such contacts are anticipated to give rise to intermolecular antiferromagnetic coupling between pairs of molecules A and B within 1D chain

We carried out DFT calculations, based upon the broken symmetry approach, at the fixed X-ray geometry for molecules A and B forming dimers I (AB) and II (BA) as well as trimers (ABA and BAB),[18,34] to determine the values of J'/k. The computed J'/k are summarized in Table 3.

The agreement between the computed values of J'/k and the experimental $J'/k = –14$ K is reasonable, especially when accuracy of the DFT computations is considered.[35] Also, while the alternating chain of J'/k may not be excluded, it is predicted by computation that the degree of alternation is relatively small and in agreement with the experiment.

Stability.

Diradical **2** possesses excellent stability at ambient conditions, not only in air-saturated solution at ambient conditions (Fig. S4, SI) but also on silica gel. Notably, solid **2** shows no signs of decomposition after storing on air at –20 °C for more than 2 years. In addition, solid **2** shows remarkable stability under vacuum annealing at 100 °C for 24 h, and we found that such condition effectively removes the solvent of crystallization (CH_2Cl_2) from the crystal lattice (SI, Fig. S6). Thus, the annealed polycrystalline **2** is obtained for the EPR spectroscopy (Figure 3) and other studies, including TGA (Figure 7), as well as for thin films (Figure 8). Thermogravimetric analysis data suggest that thermal decomposition of **2** starts at 160 °C, at a temperature that is about 15 °C lower than that for diradical **1** (Figure 7).

Thin films of 2 on SiO2/Si(111) substrate.

We test the robustness of diradical **2** toward evaporation. This aspect is important in view of the potential applications of this diradical in electronics. The ability to attach a molecule to a contact or to evaporate it onto a substrate, without degradation, is a requirement for device fabrication. Controlled evaporation of diradicals is considered very challenging, and not yet reported in literature. The presence of two radical sites, in particular the cross-conjugated diradicals with significant spin density within the π-system connecting two radical sites, such as in **2**, could potentially increase their instability during evaporation.[36]

We prepare thin films of diradical **2** on SiO_2/Si(111) wafers by using organic molecular beam deposition (OMBD) that allows for controlled evaporation and the consequent deposition of molecules onto a substrate, tuning the preparation conditions in ultra-high vacuum (UHV).[37] We investigate the films by using X-ray photoelectron spectroscopy (XPS). XPS is an effective and powerful tool for investigation of organic and organic radical thin films.[38] Besides providing insight into the occupied states, it is element-sensitive, and it can also deliver quantitative information on the stoichiometric composition of the films,[39] due to the high sensitivity of the signal to the concentration of the emitting atoms. In addition, the features contributing to the spectroscopic lines are sensitive to the different chemical environment of the atoms of the same element. These assets are the basis for our analysis of core level spectra of a multilayer of **2** (Figure 8).

We focus on the C 1s and N 1s spectra, because the O 1s spectrum is a convolution of the substrate and the molecule signal making the analysis less reliable. The film C 1s spectrum is characterized by a main line at around 285 eV due to photoelectrons emitted from the atoms in the aromatic ring and the carbon atoms bound to hydrogen atoms (C-C, C-H and CH_3). The shoulder at higher binding energy is due to contributions from the electrons emitted from carbon atoms bound also to nitrogen (C-N). Nitrogen atoms, because of their higher electronegativity, shift the electronic cloud. Thus, the carbon atoms bound to nitrogen atoms have smaller electron density and, consequently, the electrons are emitted with lower kinetic energy, i.e., higher binding energy. The N 1s core level spectrum shows contributions due to five nitrogen atoms: the three nitrogen atoms belonging to the Blatter radical have different chemical environment,[40,41] while the two nitrogen atoms belonging to the nitronyl nitroxide (NN) radical have an equivalent chemical environment. These differences are

mirrored in the spectrum by the presence of two broad features, showing the highest intensity at around 402 eV. This binding energy corresponds to the line expected in the NN radical N 1s core level spectrum.[42]

A best fit procedure allows identifying the contributions from different atomic sites having slightly different binding energies due to variations in the chemical environment.[43] In calculating the best fit, we applied several constraints based on electronegativity, and bond strength[42,43] (see also Supporting Information for details). We used Voigt profiles, with fixed constant Lorentzian width (0.08 and 0.10 eV, for C 1s and N 1s curves, respectively).[42–44] The Voigt profile takes into account both the finite core-hole lifetime (Lorentzian profile) and the broadening due to the finite experimental resolution and various inhomogeneities, e.g., molecular packing and local morphology[43,45] (Gaussian profile). To calculate the stoichiometry of the films, we also took into account the intensity of the satellites[43,44] typical features in photoemission that appear as an effect of the relaxation processes due to the creation of a core-hole.[46] Based on comparison of the film fit results (SI: Tables S4 – S6) and the molecule stoichiometry, we can conclude that there was no degradation of the diradical molecules under our controlled evaporation condition.

This result is further supported by the XPS investigations performed on the powder samples, i.e., on molecules that did not undergo evaporation (Figure 8, bottom plots). Apart from a broadening of the lines and small energy shifts, due to typical charging effects occurring in organic crystals,[47] the film spectra are fully concomitant with the powder spectra. Thus, it is evident that diradical **2** is stable and robust to be evaporated under controlled conditions to form films of intact diradical molecules.

To shed light on the growth mode of diradical **2** under this preparation conditions, we follow the XPS core level signal of the substrate (Si 2p) by looking at its attenuation upon film deposition (Figure 9, top panel). The curve is characterised by a very slow decay. This intensity trend hints at a Volmer-Weber (VW) growth mode, i.e., island growth.[48] This result is consistent with the atomic force microscopy (AFM) ex-situ images obtained on diradical **2** films (Figure 9 middle panel) clearly showing a film morphology dominated by islands. The VW growth mode occurs when the the interaction between the deposited molecules is much stronger than between the molecules and the substrate. The VW growth of diradical **2** signifies the interacting molecules of diradical **2**, possibly resembling the 1D spin-1 chain in the solid state, on the inert SiO_2/Si(111) surfaces. The line profile (Figure 9, bottom panel), obtained averaging the AFM signal over all rows, evidences the formation of islands of different lateral size that for big assemblies ranges between 80 and 300 nm.

Near edge X-ray absorption fine structure (NEXAFS) spectroscopy offers the advantage to investigate in-situ not only the electronic structure of a material, namely the unoccupied states, but also the structural properties of very thin films. Thus, we investigate diradical **2** thin films to determine the molecular orientation with respect to the substrate, by using two different polarization directions of the incident light, giving rise to NEXAFS dichroism (Figure 10).

We focus on the C-K edge spectra. In analogy with the NEXAFS spectra of carbon-based molecules, the spectra in Figure 10 are characterized by two main regions: the π* region up to around 290 eV and the σ* region in the photon energy range above 290 eV.[50] Several features are typically expected in the 286.0–287.4 eV photon range in the spectra of N-substituted aromatic carbon:[51] indeed, a strong resonance is visible at 286.2 eV. This resonance is due to transitions from C 1s levels, belonging to carbon atoms bound to nitrogen.[52–54] We also observe a very pronounced shoulder with two small knees at 284.4 and 285.2 eV. They have a C=C character, with the first shoulder mainly due to excitations along the molecular backbone and the intensity at around 285 eV within the phenyl groups.[50,55–57] The features show a strong dichroic behavior with the signal intensity at around 285 eV quenched and the peak at 286.2 eV losing intensity in normal incidence. First, this clearly indicate that the island aggregation is not amorphous because in that case the signal for the two polarization directions would overlap. Second, this kind of NEXAFS dichroism agrees with an average orientation of the molecules in the film (note that the NEXAFS signal is averaged on the area spotted by the photon beam) similar to the one adopted in the single crystals and with the crystallographic *a*-axis of the unit cell almost perpendicular to the substrate (see Figure 2).

Finally, we monitor the stability of the films in UHV (base pressure 2×10^{-10} mbar) by using XPS, focusing on the N 1s core level spectra that represent nitronyl nitroxide and Blatter radicals.[40–42] We observe no major changes in the spectra of the films after their exposure to UHV at room temperature for 17 and 60 h (Fig. S20, SI). However, the films are much less robust in air, as we observed major changes in their XPS after 7 h of air exposure (Fig. S21, SI). We note that the previously studied films of nitronyl nitroxide and the Blatter monoradical derivatives showed similar changes in their XPS after the films were kept for several weeks and several months at ambient conditions, respectively.[40–42,58] While we have demonstrated that it is possible to evaporate diradicals and deposit their thin films under controlled conditions without degradation, our results indicate that the diradical films are less stable when compared to the films of their monoradical analogues.

CONCLUSION

We have synthesized an organic diradical **2**, which, at room temperature, exists nearly exclusively in its high-spin, $S = 1$, ground state and it possesses a remarkable thermal stability to permit fabrication of intact diradical thin films on silicon substrate via evaporation under ultra-high vacuum. The diradical molecules form islands on the substrate with molecules stacked approximately along the crystallographic *a*-axis. The diradical films were found to stable under ultra-high vacuum for at least 60 h, however, within few hours of exposure to air, XPS of the films showed major changes. While we have demonstrated that it is possible to evaporate diradicals and deposit their thin films under controlled conditions without degradation, our results indicate that the diradical films are less stable when compared to the films of nitronyl nitroxide or Blatter monoradicals. Polycrystalline diradical **2** consists of nearly isotropic 1-D antiferromagnetic $S = 1$ Heisenberg chains at low temperature. Notably, **2** possesses record intra-chain antiferromagnetic coupling, $J'/k = -14$ K, among all to date studied $S = 1$ chains of organic radicals,[18,20] with a Haldane gap of $0.41 \times 2|J'/k| \approx 11.5$ K. The 1D chain of **2** is also most isotropic, with very weak local

anisotropy, $|D/2J'| \approx 4 \times 10^{-4}$,[59] and thus is potentially an excellent system for studies of low dimensional magnetism.[60] Such diradical with an unprecedented combination of novel magnetic and thermal properties, suitable for thin film fabrication under ultra-high vacuum, could facilitate the development of purely organic magnetic and electronic materials.

EXPERIMENTAL SECTION

Frozen solution EPR spectra were obtained using a Bruker EMX or EMX-plus X-band spectrometer and simulated with the EasySpin software.[28] The TGA/DSC or TGA instrument (TA Instruments TGA 550) was run either without or with IR attachment (Thermo NICOLET Is50 NIR). Variable temperature (from 1.8 K to up to 370 K) magnetic susceptibility measurements of **1** and **2** were performed using a Quantum Design SQUID magnetometer with applied magnetic fields of 30 000, 5000, and 500 Oe. Variable field (0 – 50,000 Oe) magnetization studies were carried out at temperatures of 1.8 – 5 K. Sample tubes for SQUID studies in dilute matrices are described in the SI.[61]

X-ray crystallography.

Crystals of **2** for X-ray studies was prepared by slow evaporation from solution in DCM/cyclohexane. Data collection was performed at the Advanced Photon Source, Argonne National Laboratory using λ = 0.41328 Å synchrotron radiation (silicon monochromators). Final cell constants were calculated from the xyz centroids of 9989 strong reflections from the actual data collection after integration (SAINT).[62] The intensity data were corrected for absorption (SADABS).[63] The space group P-1 was determined based on intensity statistics and the lack of systematic absences. The structure was solved and refined using the SHELX suite of programs.[64] All non-hydrogen atoms were refined with anisotropic displacement parameters. The hydrogen atoms were placed in ideal positions and refined as riding atoms with relative isotropic displacement parameters. Crystal and structure refinement data for **2** are in the Supporting Information and the accompanying file in CIF format.

Synthesis of 2.

Standard techniques for synthesis under inert atmosphere (argon or nitrogen), using custom-made Schlenk glassware, custom-made double manifold high vacuum lines, argon-filled Vacuum Atmospheres gloveboxes, and nitrogen-filled glovebags. Chromatographic separations were carried out using normal phase silica gel. Multi-step, efficient synthesis and characterization of the starting Blatter radical **3** is outlined in the Supporting Information (Scheme S1).

Blatter radical 4.—Starting 7-cyano Blatter radical **3** (1.605 g, 5.19 mmol) was dissolved in dichloromethane (100 mL) and cooled to –78 °C under a light N_2 flow. DIBAL-H (1 M in hexane, 12.0 mL, 12.0 mmol) was then added to the solution at –78 °C. The reaction was stirred at –78 °C for one hour and then warmed to room temperature with stirring for one hour. Then, 1 M HCl (100 mL) was added and the bilayer was stirred at room temperature for about 20 min. This caused a sizeable amount of precipitate to collect on the walls of the round bottom flask. The bilayer was decanted, separated, and the organic layer was shaken vigorously with aqueous KOH. The organic layer was then dried over Na_2SO_4 and

evaporated (0.634 g); TLC indicated this solid to be radical **4** with only very minor impurities. The precipitate that was formed after HCl addition was then exposed to concentrated KOH and dichloromethane, causing it to dissolve in the organic layer upon mixing. TLC indicated a sizeable amount of target material **4**, but with significantly more impurities. The solvent was evaporated and this residue purified on silica (dichloromethane eluent) to yield an additional 0.199 g of pure radical, to provide total of 0.833 g of **4** (52% yield). IR (powder, cm^{-1}): 3072, 3018, 2825, 2756, 2727, 1682, 1572, 1487, 1386, 1311, 1184, 1114, 1026, 829, 768. EPR (X-band, 9.65 GHz, benzene): $g = 2.0035$, $a_{N1} = 0.77$ mT, $a_{N2} = 0.48$ mT, $a_{N3} = 0.46$ mT. HR-ESI: 313.1229, 100%, $[M+H]^+$, calculated for $[M+H]^+$: 313.1215, also: 312.1136, 77%, M^+, calculated for M^+: 312.1137. M.p. (DSC, 5 °C/min): 212–217 °C. To further characterize radical **4** by diamagnetic NMR spectroscopy, **4** (~4 mg) was dissolved in DMSO-d_6 (~0.5 mL), and then an excess of sodium dithionite was added to the NMR sample. Gently heating the NMR tube (to dissolve enough sodium dithionite to reduce the radical to *leuco*-triazine) caused a color change to the characteristic yellow of the reduced radical. This allowed for acquisition of ^{1}H NMR and ^{13}C NMR spectra for the *leuco*-triazine. ^{1}H NMR (400 MHz, DMSO-d_6): 9.56 (s, 1H), 9.34 (s, 1H), 7.82 (dd, 2H, J_1 = 7.8 Hz, J_2 = 1.4 Hz), 7.43–7.51 (m, 7H), 7.33 (dd, J_1 = 7.8 Hz J_2 = 1.4 Hz), 7.22–7.18 (m, 1H), 6.86 (d, 1H, 7.6 Hz), 6.68 (s, 1H). ^{13}C NMR (DMSO-d_6): δ = 190.6, 146.4, 143.3, 140.5, 135.1, 132.2, 130.7, 130.4, 129.53, 129.34, 128.5, 125.9, 124.6, 122.2, 113.1, 107.9

Diradical 2.—Note: in this procedure, the first step of reduction of radical **4** with $Na_2S_2O_4$ was omitted, that is, the second step (condensation with bis-hydroxyamine) was run directly on the radical. Blatter radical **4** (0.626 g, 0.46 mmol) was added to a Schlenk vessel followed by 2,3-bis(hydroxyamino)-2,3-dimethylbutane (0.503 g, 3.34 mmol). After purging the Schlenk vessel with nitrogen gas, MeOH (20 mL) was added. The suspension was heated to 70 °C in the Schlenk vessel overnight, during which time the mixture became homogenous. Then the solution was cooled and diluted approximately fourfold with ethyl acetate, and subsequently washed twice with brine, dried, and evaporated. The solid obtained was dissolved in dichloromethane (300 mL), and then triethylamine (2.0 mL, 14.28 mmol) was added. The solution was stirred overnight with a light air flow bubbling through the reaction. The resulatant purple/red colored solution was evaporated. The diradical was purified on silica eluting with 4:1 dichloromethane/EtOAc. Then the solid diradical was washed sequentially with 10 mL pentane, 10 mL Et_2O, and finally 10 mL MeOH; the solid was then dried under high vacuum at 100 °C in a chamber overnight, to remove any co-crystallized dichloromethane and other residual solvents (0.332 g, 38% yield). IR (powder, cm^{-1}): 3101, 3049, 2982, 2914, 1585, 1483, 1388, 1361, 1315, 1269, 1136, 823, 777, 733. HR-ESI: 439.2010, 100%, M^+, calculated for M^+: 439.2008.

Computational details.

All geometry optimizations were carried out at the UB3LYP/6–31G(d) level of theory, with obtained minima confirmed by frequency calculations. The broken-symmetry approach was applied for open-shell singlet calculations and spin contamination errors were corrected by approximate spin-projection method.[65] Computations of an intra-dimer coupling constant J'/k were carried out using dimers and trimers of **2** at X-ray geometry, using broken

symmetry approach at the UB3LYP/6–31G(d) or UB3LYP/6–311++G(d,p) levels of theory.[34,66] All calculations were performed with the Gaussian 09 program suite.[27]

Thin film growth and XPS measurements.

Thin film growth and XPS measurements were performed in an UHV system comprising a substrate preparation chamber and a dedicated OMDB chamber connected to an analysis chamber (base pressure 2×10^{-10} mbar) equipped with a monochromatic Al Kα source (SPECS Focus 500) and a SPECS Phoibos 150 hemispherical electron analyser. As a substrate, native SiO_2 grown on single-side-polished n-Si(111) wafers was used. The substrate was cleaned in an ultrasonic bath in acetone and ethanol (one hour each consecutive bath) and then annealed at around 500 K for 15 hours. The cleanness was verified by XPS. Thin films of **2** were grown in-situ by OMBD using a Knudsen cell keeping the substrate at room temperature. Powder samples were obtained embedding the powder in a passivated indium foil. The nominal thickness was determined by using the attenuation of the Si 2p XPS signal of the substrate. The spectra were measured at 20 eV pass energy, and the binding energy calibrated to the Si 2p signal at 99.8 eV. Because of the radiation-sensitivity of the diradical, beam exposure was minimized and a freshly prepared film was used for each set of spectra to prevent radiation damage. For the XPS measurements probing stability, the set of spectra was measured on the same films upon UHV or air exposure minimizing the acquisition time. The spectra have a slightly worse signal-to noise ratio to preserve the intactness of the molecules in the films.

NEXAFS measurements were performed at the third-generation synchrotron radiation source Bessy II (Berlin) at the LowDose PES end-station, installed at the PM4 beamline ($E/\Delta E$ = 6000 at 400 eV) that included substrate preparation facilities like those described above for the XPS station. The measurements were carried out in multibunch hybrid mode (ring current in top up mode = 250 mA, c_{ff} = 1.6, 100-μm exit slit). The NEXAFS spectra, measured in total electron yield, were normalized by using the clean substrate signal and the ring current into account, and then scaling all spectra to give an equal edge jump.[50,57,67] Atomic force microscopy (AFM) studies were performed under ambient conditions in tapping mode with a Digital Instruments Nanoscope III Multimode AFM. No beam-induced degradation of the samples was observed on the time scale of all discussed experiments.

Supplementary Material

Refer to Web version on PubMed Central for supplementary material.

ACKNOWLEDGMENT

We thank the National Science Foundation (NSF), Chemistry Division for support of this research under Grants No. CHE-1362454 (AR) and CHE-1665256 (AR) and the National Institutes of Health (NIGMS #R01GM124310–01 to S.R. and A.R.) for the upgrade of EPR spectrometer. NSF's ChemMatCARS Sector 15 is principally supported by the NSF/Department of Energy under grant number NSF/CHE-1346572. Use of the Advanced Photon Source was supported by the U. S. Department of Energy, Office of Science, Office of Basic Energy Sciences, under Contract No. DE-AC02–06CH11357. We also would like to thank Thomas Chassé for accessing the photoelectron laboratory at the University of Tübingen, Hilmar Adler for technical support, and Helmholtz-Zentrum Berlin (HZB) for providing beamtime at BESSY II. Financial support from the German Research Foundation (DFG) under the contract CA852/11–1 and from Helmholtz-Zentrum Berlin is gratefully acknowledged. We thank Chan Shu for thermogravimetric studies of compounds **1** and **2**, and for determining stability of **2** in solution on air.

REFERENCES

(1). Rajca A; Wongsriratanakul J; Rajca S Magnetic ordering in an organic polymer. Science 2001, 294, 1503–1505. [PubMed: 11711668]

(2). Ratera L; Veciana J Playing with organic radicals as building blocks for functional molecular materials. Chem. Soc. Rev. 2012, 41, 303–349. [PubMed: 21850355]

(3). Wingate AJ; Boudouris BW Recent advances in the syntheses of radical-containing macromolecules. J. Polym. Sci., Part A: Polym. Chem. 2016, 54, 1875–1894.

(4) (a). Rajca A Organic diradicals and polyradicals: from spin coupling to magnetism?. Chem. Rev. 1994, 94, 871–893.(b) Rajca A The Physical Organic Chemistry of Very High-Spin Polyradicals. Adv. Phys. Org. Chem. 2005, 40, 153–199.(c) Gallagher NM; Arnon Olankitwanit A; Rajca A High-Spin Organic Molecules. J. Org. Chem. 2015, 80, 1291–1298. [PubMed: 25574756]

(5) (a). Rajca A; Lu K; Rajca S High-spin polyarylmethyl polyradical: Fragment of a macrocyclic 2-strand based upon calix[4]arene rings. J. Am. Chem. Soc. 1997, 119, 10335–10345.(b) Rajca S; Rajca A; Wongsriratanakul J; Butler P; Choi S Organic Spin Clusters. Dendritic-Macrocyclic Polyarylmethyl Polyradical with Very High-Spin of S = 10 and its Derivatives: Synthesis, Magnetic Studies, and Small Angle Neutron Scattering. J. Am. Chem. Soc. 2004, 126, 6972–6986. [PubMed: 15174867] (c) Rajca A; Wongsriratanakul J; Rajca S; Cerny RL Organic Spin Clusters: Annelated Macrocyclic Polyarylmethyl Polyradicals and Polymer with Very High-Spin S = 6 – 18. Chem. Eur. J. 2004, 10, 3144–3157. [PubMed: 15224323] (d) Rajca A; Wongsriratanakul J; Rajca S Organic Spin Clusters: Macrocyclic-Macrocyclic Polyarylmethyl Polyradicals with Very High-Spin S = 5 – 13. J. Am. Chem. Soc. 2004, 126, 6608–6626. [PubMed: 15161289]

(6). Sanvito S Molecular spintronics. Chem. Soc. Rev. 2011, 40, 3336–3355. [PubMed: 21552606]

(7) (a). Herrmann C; Solomon GC; Ratner MA Organic Radicals as Spin Filters. J. Am. Chem. Soc. 2010, 132, 3682–3684. [PubMed: 20192192] (b) Hu G; Xie S; Wang C; Timm C Spin-dependent transport and functional design in organic ferromagnetic devices. Beilstein J Nanotechnol. 2017, 8, 1919–1931. [PubMed: 29046839]

(8). Gaudenzi R; Burzuri E; Reta D; Moreira I. de P. R.; Bromley ST; Rovira C; Veciana J; van der Zant HSJ Exchange Coupling Inversion in a High-Spin Organic Triradical Molecule. Nano Lett. 2016, 16, 2066–2071. [PubMed: 26862681]

(9) (a). Yonekuta Y; Susuki K; Oyaizu K; Honda K; Nishide H Battery-Inspired, Nonvolatile, and Rewritable Memory Architecture: a Radical Polymer-Based Organic Device. J. Am. Chem. Soc. 2007, 129, 14128–14129. [PubMed: 17963388] (b) Oyaizu K; Nishide H Radical Polymers for Organic Electronic Devices: A Radical Departure from Conjugated Polymers? Adv. Mater. 2009, 21, 2339–2344.(c) Lee J; Lee E; Kim S; Bang GS; Shultz DA; Schmidt RD; Forbes MDE; Lee H Nitronyl Nitroxide Radicals as Organic Memory Elements with Both n- and p-Type Properties. Angew. Chem. Int. Ed. 2011, 50, 4415–4418.(d) Gaudenzi R; Bruijckere J; Reta D; Moreira I. de P. R.; Rovira C; Veciana J; van der Zant HSJ; Burzurí E Redox-Induced Gating of the Exchange Interactions in a Single Organic Diradical. ACS Nano 2017, 11, 5879–5883. [PubMed: 28494146]

(10). Tsuji Y; Hoffmann R; Strange M; Solomon GC Close relation between quantum interference in molecular conductance and diradical existence. Proc. Natl. Acad. Sci. U. S. A. 2016, 113, E413–E419. [PubMed: 26755578]

(11). Borden WT; Davidson ER Effects of electron repulsion in conjugated hydrocarbon diradicals. J. Am. Chem. Soc. 1977, 99, 4587–4594.

(12). Ovchinnikov AA Multiplicity of the ground state of large alternant organic molecules with conjugated bonds (do organic ferromagnets exist?). Theor. Chim. Acta 1978, 47, 297–304.

(13) (a). Boratyński PJ; Pink M; Rajca S; Rajca A Isolation of the Triplet Ground State Aminyl Diradical. Angew. Chem., Int. Ed. 2010, 49, 5459–5462.(b) Rajca A; Olankitwanit A; Wang Y; Boratynski PJ; Pink M; Rajca S High-Spin S = 2 Ground State Aminyl Tetraradicals. J. Am. Chem. Soc. 2013, 135, 18205–18215. [PubMed: 24251582] (c) Shimizu D; Osuka A A Benzene-1,3,5-Triaminyl Radical Fused with Zn-II-Porphyrins: Remarkable Stability and a High-Spin Quartet Ground State. Angew. Chem. Int. Ed. 2018, 57, 3733–3736.

(14). Fukuzaki E; Nishide H Room-temperature high-spin organic single molecule: nanometer-sized and hyperbranched poly[1,2,(4)-phenylenevinyleneanisylaminium]. J. Am. Chem. Soc. 2006, 128, 996–1001. [PubMed: 16417391]

(15) (a). Ishida T; Iwamura H Bis[3-tert-butyl-5-(N-oxy-tert-butylamino)phenyl] nitroxide in a quartet ground state: a prototype for persistent high-spin poly[(oxyimino)-1,3-phenylenes]. J. Am. Chem. Soc. 1991, 113, 4238–4241.(b) Veciana J; Rovira C; Crespo MI; Armet O; Domingo VM; Palacio F Stable polyradicals with high-spin ground states. 1. synthesis, separation, and magnetic characterization of the stereoisomers of 2,4,5,6-tetrachloro-α,α,α′,α′-tetrakis(pentachloropheny1)-m-xylylene. J. Am. Chem. Soc. 1991, 113, 2552–2561.(c) Rajca A; Shiraishi K; Rajca S Stable diarylnitroxide diradical with triplet ground state. Chem. Commun. 2009, 4372–4374

(16) (a). Inoue K; Iwamura H 2-[p-(N-tert-butyl-N-oxyamino)phenyl]-4,4,5,5-tetramethyl-4,5-dihydroimidazol-3-oxide-l-oxyl, a stable diradical with a triplet ground state. Angew. Chem. Int. Ed. 1995, 34, 927–928.(b) Shultz DA; Fico RM; Lee H; Kampf JW; Kirschbaum K; Pinkerton AA; Boyle PD Mechanisms of exchange modulation in trimethylenemethane-type biradicals: The roles of conformation and spin density. J. Am. Chem. Soc. 2003, 125, 15426–15432. [PubMed: 14664588] (c) Rajca A; Shiraishi K; Vale M; Han H; Rajca S Stable Hydrocarbon Diradical, an Analogue of Trimethylenemethane. J. Am. Chem. Soc. 2005, 127, 9014–9020. [PubMed: 15969578] (d) Kato K; Furukawa K; Osuka A A Stable Trimethylenemethane Triplet Diradical Based on a Trimeric Porphyrin Fused π-System. Angew. Chem. Int. Ed. 2018, 57, 9491–9494.

(17). Gallagher NM; Bauer JJ; Pink M; Rajca S; Rajca A High-spin organic diradical with robust stability. J. Am. Chem. Soc. 2016, 138, 9377–9380. [PubMed: 27430499]

(18). Wang W; Chen C; Shu C; Rajca S; Wang X; Rajca AS = 1 Tetraazacyclophane Diradical Dication with Robust Stability: a Case of Low Temperature One-Dimensional Antiferromagnetic Chain. J. Am. Chem. Soc. 2018, 140, 7820–7826. [PubMed: 29863339]

(19). Suzuki S; Furui T; Kuratsu M; Kozaki M; Shiomi D; Sato K; Takui T; Okada K Nitroxide-substituted nitronyl nitroxide and iminonitroxide. J. Am. Chem. Soc. 2010, 132, 15908–15910. [PubMed: 20964296]

(20). Rajca A; Takahashi M; Pink M; Spagnol G; Rajca S Conformationally constrained, stable, triplet ground state (S = 1) nitroxide diradicals: antiferromagnetic chains of (S = 1) diradicals. J. Am. Chem. Soc. 2007, 129, 10159–10170. [PubMed: 17655296]

(21) (a). Bodzioch A; Zheng M; Kaszyński P; Utecht G Functional Group Transformations in Derivatives of 1,4-Dihydrobenzo[1,2,4]triazinyl Radical. J. Org. Chem. 2014, 79, 7294–7310. [PubMed: 25068765] (b) Constantinides CP; Obijalska E; Kaszyński PP Access to 1,4-Dihydrobenzo[e][1,2,4]triazin-4-yl Derivatives. Org. Lett. 2016, 18, 916–919. [PubMed: 26910442]

(22). Savva AC; Mirallai SI; Zissimou GA; Berezin AA; Demetriades M; Kourtellaris A; Constantinides CP; Nicolaides C; Trypiniotis T; Koutentis. P. A. Preparation of Blatter Radicals via Aza-Wittig Chemistry: The Reaction of N-Aryliminophosphoranes with 1-(Het)aroyl-2-aryldiazenes. J. Org. Chem. 2017, 82, 7564–7575. [PubMed: 28628743]

(23). Constantinides CP; Koutentis PA Stable N- and N/S-Rich Heterocyclic Radicals: Synthesis and Applications. Adv. Heterocycl. Chem. 2016, 119, 173–207.

(24). Constantinides CP; Berezin AA; Zissimou GA; Manoli M; Leitus GM; Bendikov M; Probert MR; Rawson JM; Koutentis PA A Magnetostructural Investigation of an Abrupt Spin Transition for 1-Phenyl-3-trifluoromethyl-1,4-dihydrobenzo[e][1,2,4]triazin-4-yl. J. Am. Chem. Soc. 2014, 136, 11906–11909. [PubMed: 25093450]

(25). Berezin AA; Zissimou GA; Constantinides CP; Beldjoudi Y; Rawson JM; Koutentis PA Route to Benzo- and Pyrido-Fused 1,2,4-Triazinyl Radicals via N′-(Het)aryl-N′-[2-nitro(het)aryl]hydrazides. J. Org. Chem. 2014, 79, 314–327. [PubMed: 24350615]

(26). Rajca A; Pink M; Mukherjee S; Rajca S; Das K 1,3-Alternate calix[4]arene nitronyl nitroxide tetraradical and diradical: synthesis, X-ray crystallography, paramagnetic NMR spectroscopy, EPR spectroscopy, and magnetic studies. Tetrahedron 2007, 63, 10731–10742. [PubMed: 19568320]

(27). Frisch MJ; Trucks GW; Schlegel HB; Scuseria GE; Robb MA; Cheeseman JR; Scalmani G; Barone V; Mennucci B; Petersson GA; Nakatsuji H; Caricato M; Li X; Hratchian HP; Izmaylov

AF; Bloino J; Zheng G; Sonnenberg JL; Hada M; Ehara M; Toyota K; Fukuda R; Hasegawa J; Ishida M; Nakajima T; Honda Y; Kitao O; Nakai H; Vreven T; Montgomery JA Jr.; Peralta JE; Ogliaro F; Bearpark M; Heyd JJ; Brothers E; Kudin KN; Staroverov VN; Kobayashi R; Normand J; Raghavachari K; Rendell A; Burant JC; Iyengar SS; Tomasi J; Cossi M; Rega N; Millam NJ; Klene M; Knox JE; Cross JB; Bakken V; Adamo C; Jaramillo J; Gomperts R; Stratmann RE; Yazyev O; Austin AJ; Cammi R; Pomelli C; Ochterski JW; Martin RL; Morokuma K; Zakrzewski VG; Voth GA; Salvador P; Dannenberg JJ; Dapprich S; Daniels AD; Farkas Ö; Foresman JB; Ortiz JV; Cioslowski J; Fox DJ Gaussian 09, Revision A.1 (Gaussian, Inc., Wallingford CT, 2009).

(28). Stoll S; Schweiger A EasySpin, a comprehensive software package for spectral simulation and analysis in EPR. J. Magn. Reson. 2006, 178, 42–55. [PubMed: 16188474]

(29). Neese F ORCA—An Ab Initio, Density Functional and Semiempirical Program Package, version 3.0.1; University of Bonn, Germany, 2008.

(30) (a). Rajca A; Olankitwanit A; Rajca S Triplet Ground State Derivative of Aza-m-Xylylene Diradical with Large Singlet−Triplet Energy Gap. J. Am. Chem. Soc. 2011, 133, 4750–4753. [PubMed: 21401132] (b) Olankitwanit A; Pink M; Rajca S; Rajca A Synthesis of Aza-m-Xylylene Diradicals with Large Singlet-Triplet Energy Gap and Statistical Analyses of their EPR Spectra. J. Am. Chem. Soc. 2014, 136, 14277–14288. [PubMed: 25216763] (c) Olankitwanit A; Rajca S; Rajca A Aza-m-Xylylene Diradical with Increased Steric Protection of the Aminyl Radicals. J. Org. Chem. 2015, 80, 5035–5044. [PubMed: 25901647]

(31). Sinnecker S; Neese F Spin−Spin Contributions to the Zero-Field Splitting Tensor in Organic Triplets, Carbenes and Biradicals - A Density Functional and Ab Initio Study. J. Phys. Chem. A 2006, 110, 12267–12275. [PubMed: 17078624]

(32). Meyer A; Gleizes A; Girerd JJ; Verdaguer M; Kahn O Crystal structures, magnetic anisotropy properties, and orbital interactions in catena - (μ-nitrito) - bis (ethylenediamine) nickel(II) perchlorate and triiodide. Inorg. Chem. 1982, 21, 1729–1739.

(33). Beloritzky E; Fries PH Exact solutions for simple spin clusters with isotropic Heisenberg exchange interactions. J. Chim. Phys. (Paris) 1993, 90, 1077–1100.

(34). Sadhukhan T; Hansda S; Latif IA; Datta SN Metaphenylene-Based Nitroxide Diradicals: A Protocol to Calculate Intermolecular Coupling Constant in a One-Dimensional Chain. J. Phys. Chem. A 2013, 117, 13151–13160. [PubMed: 24266400]

(35). Cho Y; Cho WJ; Youn S; Lee G; Singh NJ; Kim KS Density Functional Theory Based Study of Molecular Interactions, Recognition, Engineering, and Quantum Transport in π Molecular Systems. Acc. Chem. Res. 2014, 47, 3321–3330. [PubMed: 25338296]

(36). Huang Z; Zhang Y; He Y; Song H; Yin C; Wu K A chemist's overview of surface electron spins. Chem. Soc. Rev. 2017, 46, 1955–1976. [PubMed: 28317957]

(37). Forrest SR Ultrathin Organic Films Grown by Organic Molecular Beam Deposition and Related Techniques. Chem. Rev. 1997, 97, 1793–1896. [PubMed: 11848893]

(38). Casu MB Nanoscale Studies of Organic Radicals: Surface, Interface, and Spinterface. Acc. Chem. Res. 2018, 51, 753–760. [PubMed: 29465979]

(39). Casu MB; Chassé T Photoelectron Spectroscopy Applications to Materials Science. Second ed.; Wiley-VCH: Weinheim, 2014.

(40). Ciccullo F; Gallagher NM; Geladari O; Chasse T; Rajca A; Casu MB A Derivative of the Blatter Radical as a Potential Metal-Free Magnet for Stable Thin Films and Interfaces. ACS Appl. Mater. Interfaces 2016, 8, 1805–1812. [PubMed: 26727145]

(41). Ciccullo F; Calzolari A; Bader K; Neugebauer P; Gallagher NM; Rajca A; van Slageren J; Casu MB, Interfacing a Potential Purely Organic Molecular Quantum Bit with a Real-Life Surface. ACS Appl. Mater. Interfaces 2019, 11, 1571–1578. [PubMed: 30520295]

(42). Savu S-A; Biswas I; Sorace L; Mannini M; Rovai D; Caneschi A; Chassé T; Casu MB Nanoscale Assembly of Paramagnetic Organic Radicals on Au(111) Single Crystals. Chem.-Eur. J. 2013, 19, 3445–3450. [PubMed: 23355391]

(43). Savu S-A; Casu MB; Schundelmeier S; Abb S; Tonshoff C; Bettinger HF; Chassé T Nanoscale assembly, morphology and screening effects in nanorods of newly synthesized substituted pentacenes. RSC Adv. 2012, 2, 5112–5118.

(44). Schöll A; Zou Y; Jung M; Schmidt T; Fink R; Umbach E Line Shapes and Satellites in High-Resolution X-Ray Photoelectron Spectra of Large Π-Conjugated Organic Molecules. J. Chem. Phys. 2004, 121, 10260–10267. [PubMed: 15549902]

(45). Casu MB; Schuster B-E; Biswas I; Raisch C; Marchetto H; Schmidt T; Chassé T Locally Resolved Core-Hole Screening, Molecular Orientation, and Morphology in Thin Films of Diindenoperylene Deposited on Au(111) Single Crystals. Adv. Mater. 2010, 22, 3740–3744. [PubMed: 20549709]

(46). Sjögren B; Svensson S; de Brito AN; Correia N; Keane MP; Enkvist C; Lunell S The C1s core shake-up spectra of alkene molecules: An experimental and theoretical study. J. Chem. Phys. 1992, 96, 6389–6398.

(47). Barth G; Linder R; Bryson C Advances in charge neutralization for XPS measurements of nonconducting materials. Surf. Interface Anal. 1988, 11, 307–311.

(48). Bauer E, Phänomenologische Theorie Der Kristallabscheidung an Oberflächen. I. Z. Kristallogr. 1958, 110, 372–394.

(49). Venables JA, Introduction to Surface and Thin Film Processes. Cambridge University Press: Cambridge, 2000.

(50). Stöhr J, NEXAFS Spectroscopy. Springer: 2003.

(51). Synchrotron-Based near-Edge X-Ray Spectroscopy of Natural Organic Matter in Soils and Sediments. In Biophysico-Chemical Processes Involving Natural Nonliving Organic Matter in Environmental Systems.

(52). Shen C; Haryono M; Grohmann A; Buck M; Weidner T; Ballav N; Zharnikov M, Self-Assembled Monolayers of a Bis(Pyrazol-1-Yl)Pyridine-Substituted Thiol on Au(111). Langmuir 2008, 24, 12883–12891. [PubMed: 18950209]

(53). Zubavichus Y; Shaporenko A; Korolkov V; Grunze M; Zharnikov M, X-Ray Absorption Spectroscopy of the Nucleotide Bases at the Carbon, Nitrogen, and Oxygen K-Edges. The Journal of Physical Chemistry B 2008, 112, 13711–13716. [PubMed: 18842017]

(54). Kelly DN; Schwartz CP; Uejio JS; Duffin AM; England AH; Saykally RJ, Communication: Near Edge X-Ray Absorption Fine Structure Spectroscopy of Aqueous Adenosine Triphosphate at the Carbon and Nitrogen K-Edges. The Journal of Chemical Physics 2010, 133, 101103. [PubMed: 20849154]

(55). Käfer D; Ruppel L; Witte G; Wöll C, Role of Molecular Conformations in Rubrene Thin Film Growth. Phys. Rev. Lett. 2005, 95, 166602.

(56). Casu MB; Schuster B-E; Biswas I; Raisch C; Marchetto H; Schmidt T; Chassé T, Locally Resolved Core-Hole Screening, Molecular Orientation, and Morphology in Thin Films of Diindenoperylene Deposited on Au(111) Single Crystals. Adv. Mater. 2010, 22, 3740–3744. [PubMed: 20549709]

(57). Casu MB, Nanoscale Order and Structure in Organic Materials: Diindenoperylene on Gold as a Model System. Cryst. Growth Des. 2011, 11, 3629–3635.

(58). Kakavandi R; Ravat P; Savu SA; Borozdina YB; Baumgarten M; Casu MB, Electronic Structure and Stability of Fluorophore–Nitroxide Radicals from Ultrahigh Vacuum to Air Exposure. ACS Appl. Mater. Interfaces 2015, 7, 1685–1692. [PubMed: 25522370]

(59). Zheludev A; Chen Y; Broholm CL; Honda Z; Katsumata K Haldane-gap excitations in the low-Hcone-dimensional quantum antiferromagnet Ni(C5D14N2)2N3(PF6). Phys. Rev. B: Condens. Matter Mater. Phys. 2001, 63, 104410.

(60). (a) Wierschem K; Sengupta P Quenching the haldane gap in spin-1 Heisenberg antiferromagnets. Phys. Rev. Lett. 2014, 112, 247203. [PubMed: 24996106] (b) Blanc N; Trinh J; Dong L; Bai X; Aczel AA; Mourigal M; Balents L; Siegrist T; Ramirez AP Quantum criticality among entangled spin chains. Nature Phys. 2018, 14, 273–276.

(61). Rajca A; Mukherjee S; Pink M; Rajca S Exchange Coupling Mediated Through-Bonds and Through-Space in Conformationally-Constrained Polyradical Scaffolds: Calix[4]arene Nitroxide Tetraradicals and Diradical. J. Am. Chem. Soc. 2006, 128, 13497–13507. [PubMed: 17031963]

(62). SAINT, Bruker Analytical X-Ray Systems, Madison, WI, current version.

(63). SADABS, Bruker Analytical X-Ray Systems, Madison, WI, current version.

(64). Sheldrick GM A short history of SHELX. Acta Cryst. A 2008, 64, 112–122. [PubMed: 18156677]

(65). Trinquier G; Suaud N; Malrieu J-P Theoretical Design of High-Spin Polycyclic Hydrocarbons. Chem. Eur. J. 2010, 16, 8762–8772. [PubMed: 20572170]

(66). Yamaguchi K; Jensen F; Dorigo A; Houk KN A Spin Correction Procedure for Unrestricted Hartree−Fock and Møller−Plesset Wavefunctions for Singlet Diradicals and Polyradicals. Chem. Phys. Lett. 1988, 149, 537–542.

(67). Casu MB; Cosseddu P; Batchelor D; Bonfiglio A; Umbach E, A High-Resolution near-Edge X-Ray Absorption Fine Structure Investigation of the Molecular Orientation in the Pentacene/Poly(3,4-Ethylenedioxythiophene):Poly(Styrenesulfonate) Pentacene/System. J. Chem. Phys. 2008, 128, 014705. [PubMed: 18190210]

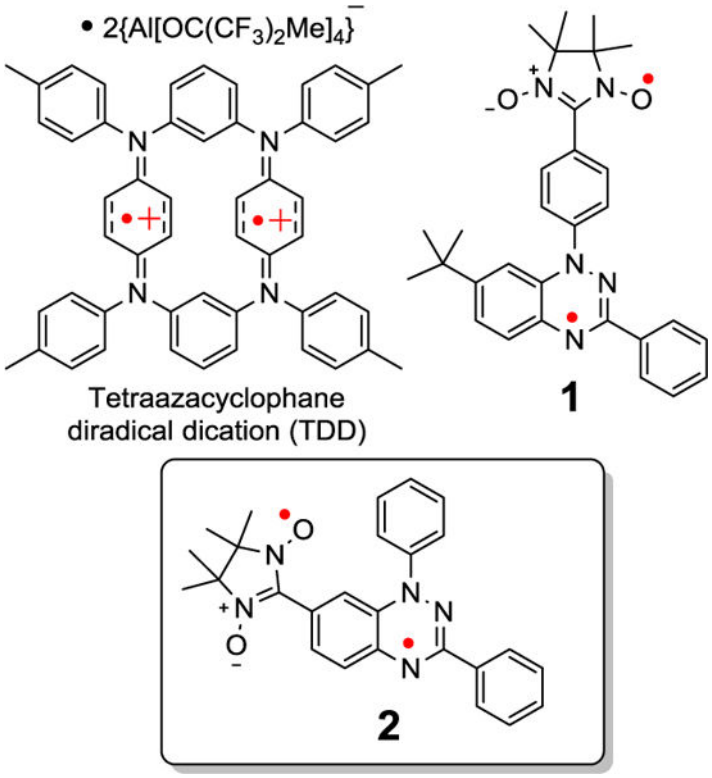

Figure 1.
Thermally robust triplet ground state diradicals with onset of decomposition at $T \geq 160$ °C based upon TGA.

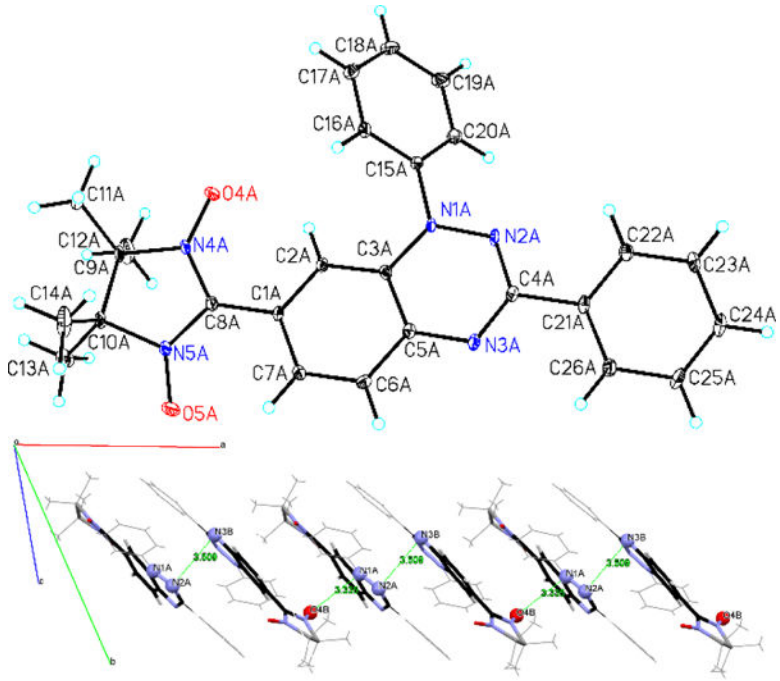

Figure 2.

Top: Single crystal X-ray structure of diradical **2** with molecule A shown only; carbon, nitrogen, and oxygen atoms are depicted with thermal ellipsoids set at the 50% probability level. Bottom: Packing of molecules A and B into a one-dimensional $S = 1$ antiferromagnetic chain; nitrogens and oxygens with large positive spin densities and forming close intermolecular contacts, N2A···N3B = 3.509 Å and O4B···N1A = 3.335 Å, are emphasized as ball-and-stick. Additional information can be found in the Supporting Information (Figs. S1-S3 and Table S1).

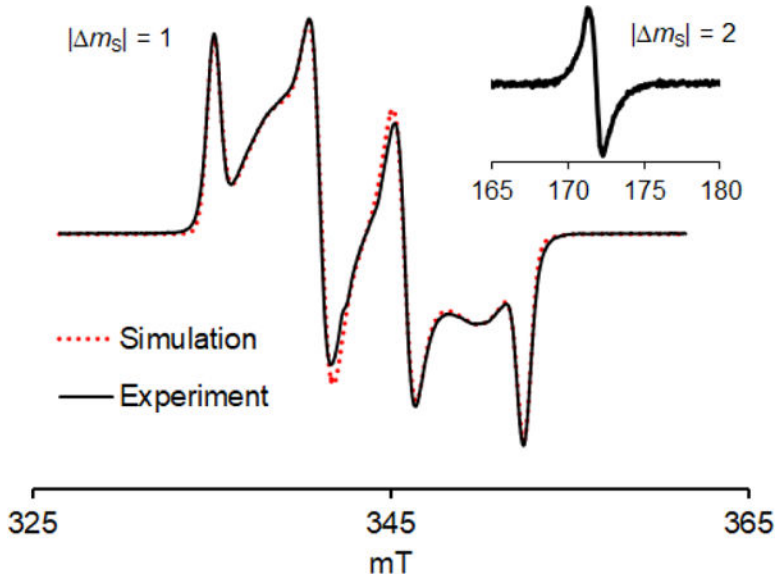

Figure 3.

EPR (ν = 9.65 GHz) spectrum of 1.2 mM diradical **2** in 4:1 toluene/chloroform glass at 153 K. The $\Delta m_s = 2$ transition is shown as an inset. Simulation parameters: $g_{xx} = 2.0072$, $g_{yy} = 2.0026$, $g_{zz} = 2.0052$, $|D/hc| = 8.08 \times 10^{-3}$ cm^{-1}, $|E/hc| = 1.17 \times 10^{-3}$ cm^{-1}; linewidths: $LW_x = 32.0$ MHz, $LW_y = 100.0$ MHz, $LW_z = 24.9$ MHz. For EPR spectra (with simulations) of **2** in polystyrene matrix at 295 K, see: SI, Fig. S7.

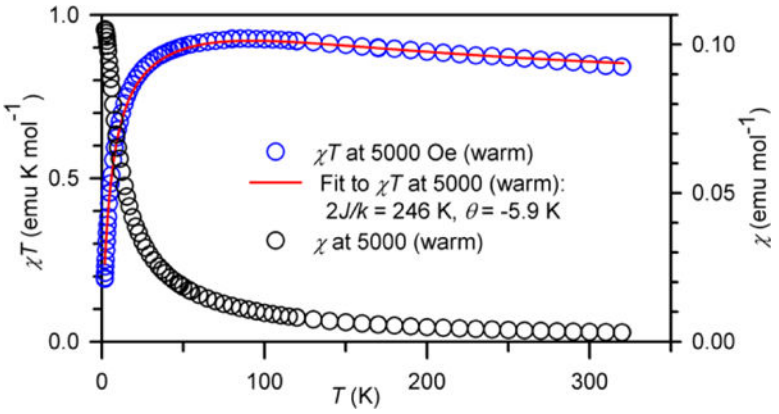

Figure 4.

SQUID magnetometry of polycrystalline (solid) diradical **1**: plots of χT vs. T and at χ vs. T at H = 5000 Oe in the warming mode. χT vs. T data, corrected for diamagnetism, are fit to a diradical model (eq. 1), using two variable parameters: singlet triplet energy gap, $2J/k$, mean-field correction for intermolecular interactions between the radicals, θ. The values of standard error, *SE*, and parameter dependence, *DEP*, are provided; goodness of fit may be measured by standard error of estimate, *SEE*. Fitting parameters: $2J/k$ = 246 K (*SE* = 8), θ = −5.89 K (*SE* = 0.08), *DEP* = 0.0236, R^2 = 0.9941, *SEE* = 0.0175. Complete set of magnetic data (and fits) for solid diradical **1** may be found in the SI (Fig. S8 and Eq. S1).

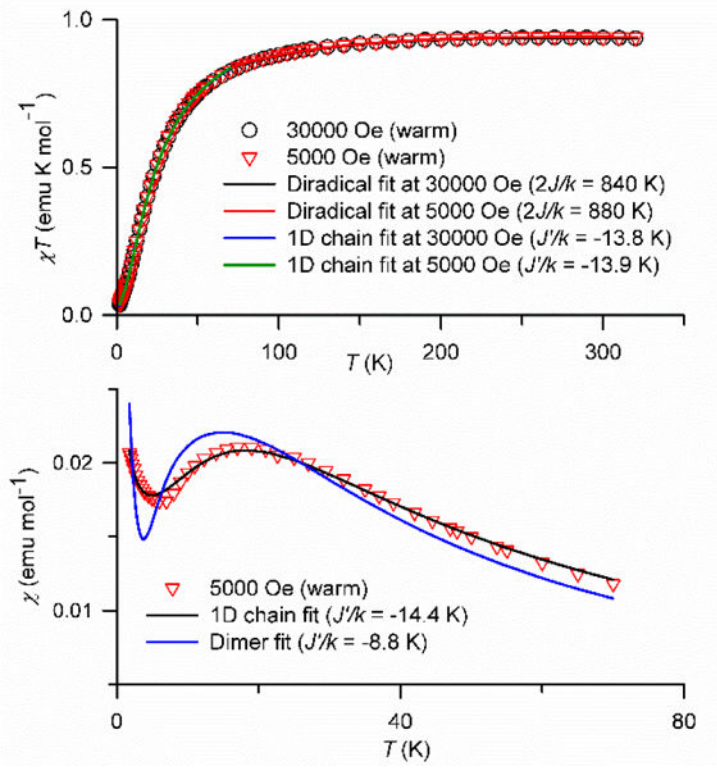

Figure 5.

SQUID magnetometry of polycrystalline (solid) diradical **2**: plots of χT vs. T and at χ vs. T at various applied magnetic fields, H = 300000 Oe and 5000 Oe in the warming mode and H = 500 Oe in the cooling mode. Numerical fits to the diradical model (eq. 1) for T = 70 – 320 K are carried out with two variable parameters: singlet triplet energy gap, $2J/k$ and mean-field correction for intermolecular interactions between the radicals, θ. Numerical fits to 1D chain (eq. 2) or dimer (eqs. S2A&B, SI) models for T = 1.8 – 70 K are carried out with three variable parameters: intermolecular Heisenberg exchange coupling constant, J'/k, weight factor, N, and weight factor for isolated S = 1 diradical, N_{imp}. The results for numerical fits are summarized in Table 2 and in the Supporting Information (Table S3 and Figs. S9 and S10).

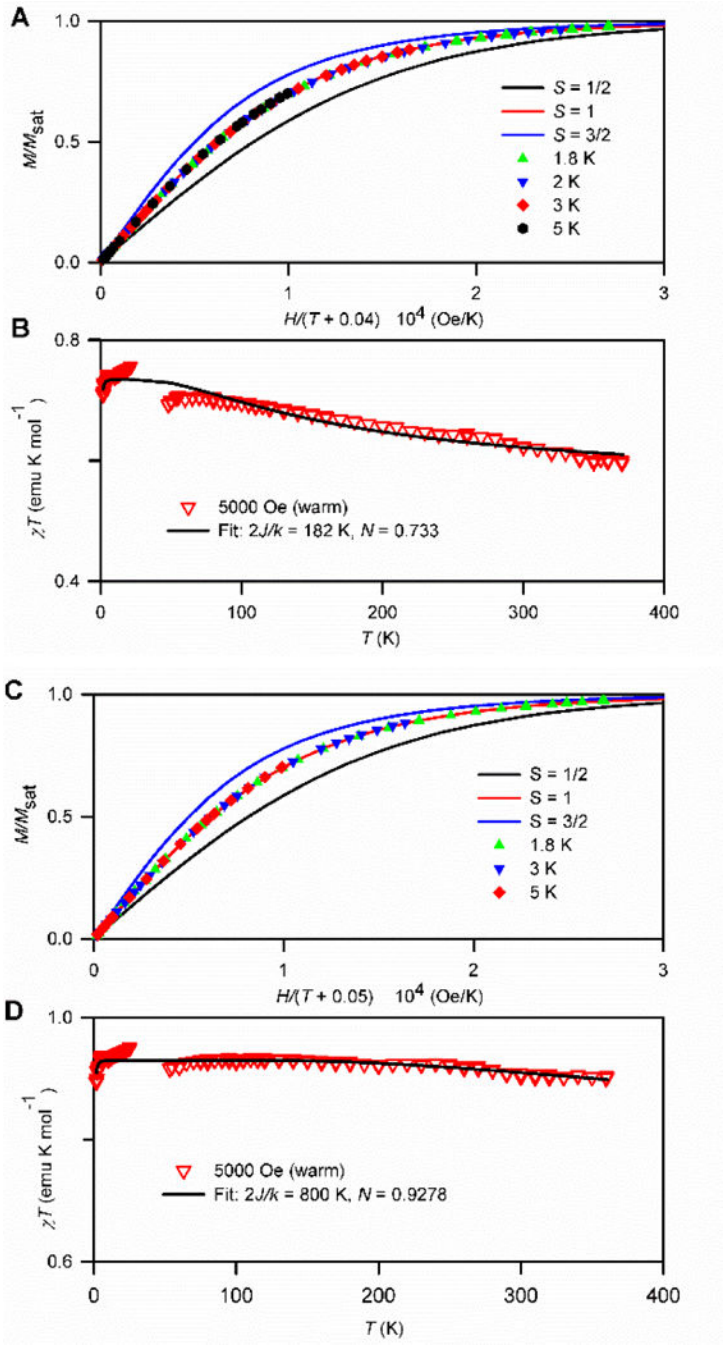

Figure 6.

SQUID magnetometry of 30 – 40 mM diradicals **1** (A & B) and **2** (C & D) in polystyrene matrix. Plots A and C: M/M_{sat} vs. $H/(T-\theta)$ plots, where $\theta = -0.04$ or -0.05 K, at $T = 1.8$ – 5 K (symbols) and the Brillouin curves corresponding to $S = ½$ - 3/2 (lines). Plots B and D: χT vs. T data at $H = 5000$ Oe in the warming mode were fit to a diradical model (eq. 1), using two variable parameters: singlet-triplet energy gap, $2J/k$, mean-field correction for intermolecular interactions between the radicals, θ. The values of standard error, *SE*, and parameter dependence, *DEP*, coefficient of determination, R^2, and standard error of

estimate, *SEE*. Fitting parameters: diradical **1**: $2J/k$ = 182 K (*SE* = 5), *N* = 0.733 (SE = 0.001), *DEP* = 0.5311, R^2 = 0.9441, *SEE* = 0.0109; diradical **2**: $2J/k$ = 800 K (*SE* = 20), *N* = 0.9278 (SE = 0.0008), *DEP* = 0.3336, R^2 = 0.746, *SEE* = 0.0066. Further details are reported in the SI: Table S3, Figs. S11 and S12.

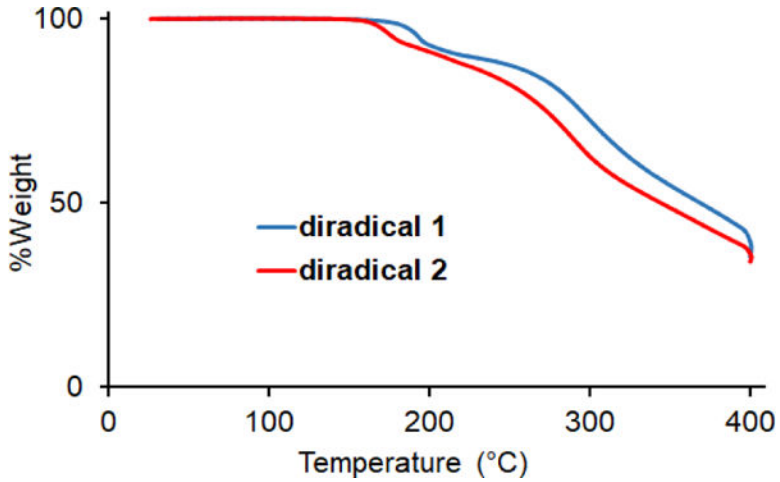

Figure 7.

Thermogravimetric analysis (TGA) of diradicals **1** and **2** under N_2; heating rate = 5 °C min–1. Further details may be found in the SI (Figs. S4-S6).

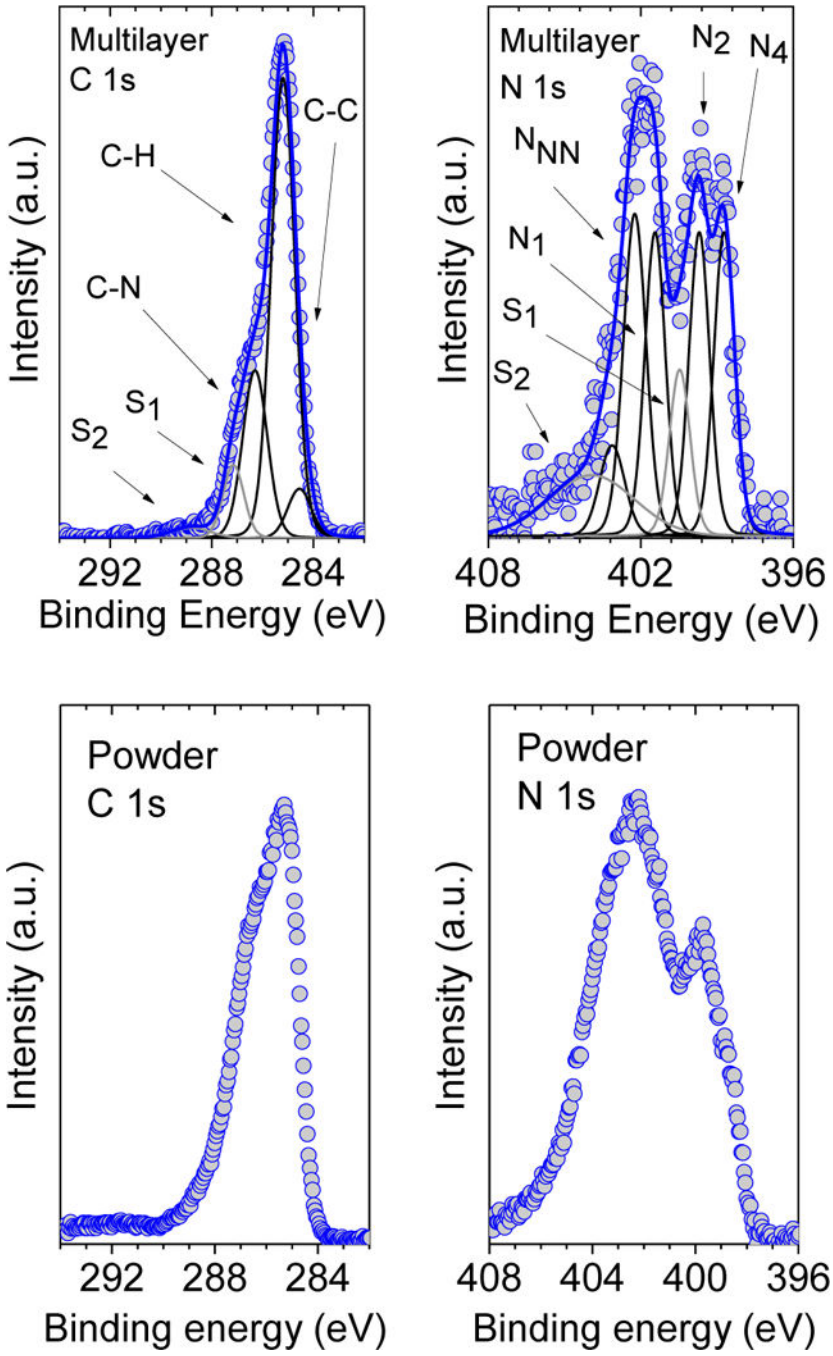

Figure 8.

C 1s and N 1s core level XPS spectra of a multilayer of diradical **2** deposited on SiO_2/Si(111) wafers (top plots), compared to the powder spectra (bottom plots).

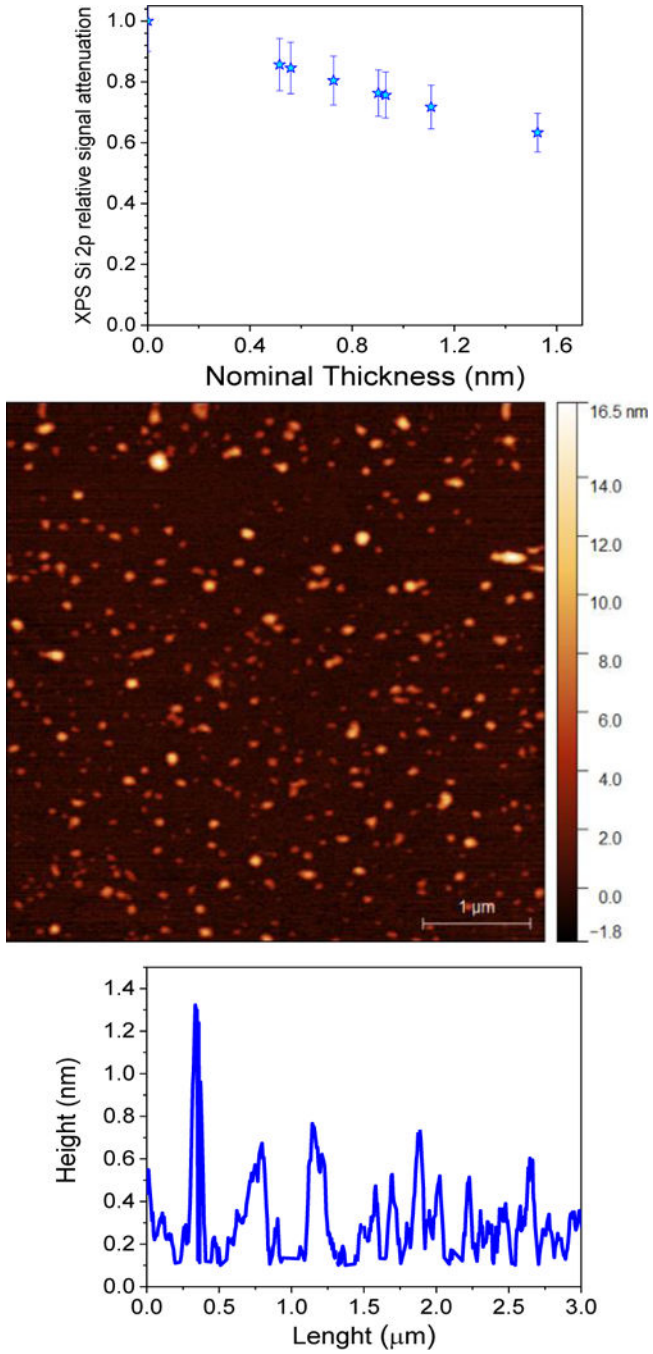

Figure 9.

Attenuation of the Si 2p XPS signal, normalized to the corresponding saturation signal, as a function of film nominal thickness, deposition at room temperature (top panel). A typical AFM image of a 1.4-nm nominally thick film (middle panel) and its averaged height profile (bottom panel).

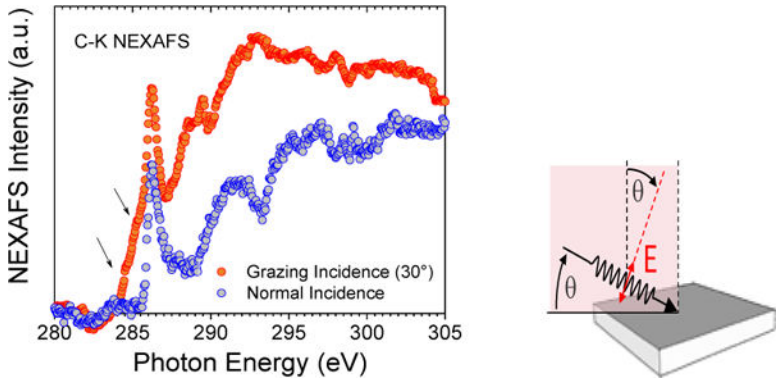

Figure 10.

C-K NEXAFS spectra obtained from a 1.5-nm nominally thick film (left panel). The spectra were taken in grazing incidence and in normal incidence as indicated. Geometry of the experiment (right panel).

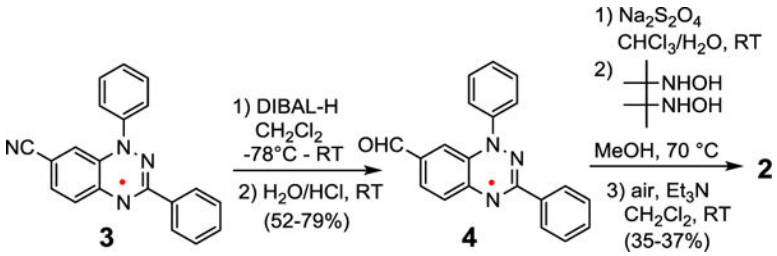

Scheme 1.
Synthesis of Diradical 2.

Table 1.

Summary of experimental and DFT-computed singlet-triplet energy gaps and selected EPR parameters for diradicals 1 and 2.

	ΔE_{ST} (kcal mol^{-1})		D/hc (10^{-3}cm^{-1})		E/hc (10^{-3}cm^{-1})		g^a	
	SQUID[b]	DFT[c]	EPR	DFT[d]	EPR	DFT[d]	EPR	DFT[d]
1	+0.50 ± 0.02	+1.4	2.32	−5.47	0.14	−1.56	2.0044	2.0053
2	+1.74 ± 0.07	+3.5	8.08	+12.0	1.17	+3.25	2.0050	2.0053

[a] Isotropic $g = (g_X + g_Y + g_Z)/3$.

[b] ΔE_{ST} is determined by SQUID of solid diradicals **1** and **2**.

[c] BS-DFT-computed ΔE_{ST} at the UB3LYP/6–31G(d,p) level[17]

[d] Computed at the B3LYP/EPR-II level using ORCA.

Table 2.

Fitting parameters for SQUID data for polycrystalline diradical 2.

	T [K]	*Fit*	*H* [Oe]	2*J*/*k* or *J*′/*k* (*SE*, *DEP*) [a] [K]	*θ* (*SE*, *DEP*) [b] [K]	*N* (*SE*, *DEP*) [c]	*SEE* [d]	R^2 [e]
χT	70–320	Diradical	30000	844 (14, 0.178)	−14.05 (0.08, 0.178)	NA	0.0028	0.9933
			5000	878 (16, 0.172)	−13.87 (0.09, 0.172)	NA	0.0029	0.9926
	1.8–70	1D-chain	30000	−13.87 (0.06, 0.902)	0.48 (0.03, 0.701)	1.093 (0.002, 0.842)	0.0026	0.9999
			5000	−14.00 (0.07, 0.903)	0.48 (0.04, 0.700)	1.100 (0.003, 0.843)	0.0030	0.9999
		Dimer	30000	−9.329 (0.23, 0.767)	1.33 (0.03, 0.308)	0.97 (0.01, 0.725)	0.0240	0.9927
			5000	−9.590 (0.25, 0.757)	1.70 (0.01, 0.228)	0.97 (0.2, 0.733)	0.0269	0.9909
χ	1.8–70	1D-chain	5000	−14.32 (0.11, 0.926)	0.52 (0.01, 0.481)	1.116 (0.008, 0.918)	0.0003	0.9871
			500	−14.00 (0.10, 0.927)	0.41 (0.01, 0.532)	1.068 (0.007, 0.917)	0.0002	0.989
		Dimer	5000	−5.49 (0.25, 0.866)	1.56 (0.02, 0.749)	0.57 (0.04, 0.676)	0.0048	-
			500	−7.73 (0.59, 0.769)	1.97 (0.01, 0.608)	0.77 (0.10, 0.562)	0.0089	-
	T [K]	*Fit*	*H* [Oe]	*J*′/*k* (*SE*, *DEP*) [a] [K]	*N* (*SE*, *DEP*) [c]	N_{imp} (*SE*, *DEP*) [f]	*SEE* [d]	R^2 [e]
χT	1.8–70	1D-chain	30000	−13.82 (0.07, 0.9080)	1.086 (0.002, 0.8328)	0.0110 (0.0010, 0.832)	0.0028	0.9999
			5000	−13.85 (0.07, 0.8920)	1.094 (0.003, 0.8333)	0.0082 (0.0009, 0.752)	0.0032	0.9999
		Dimer	30000	−10.86 (0.07, 0.8817)	0.967 (0.003, 0.7830)	0.0696 (0.0014, 0.795)	0.0043	0.9998
			5000	−10.42 (0.10, 0.8542)	0.974 (0.005, 0.7751)	0.0537 (0.0018, 0.709)	0.0067	0.9994
χ	1.8–70	1D-chain	5000	−14.43 (0.11, 0.9194)	1.117 (0.007, 0.9079)	0.0108 (0.0002, 0.485)	0.0002	0.9899
			500	−14.03 (0.08, 0.9182)	1.067 (0.006, 0.9063)	0.0077 (0.0001, 0.504)	0.0002	0.9930
		Dimer	5000	−8.75 (0.26, 0.7387)	0.861 (0.028, 0.6951)	0.044 (0.001, 0.240)	0.0017	0.4916
			500	−8.36 (0.28, 0.7173)	0.814 (0.030, 0.6845)	0.038 (0.001, 0.175)	0.0018	0.3333

[a] *J*/*k* or *J*′/*k*, Heisenberg exchange coupling constant; 2*J*/*k* = singlet triplet energy gap in Kelvin; *SE*, standard error; *DEP*, parameter dependence.

[b] *θ*, mean-field correction.

[c] *N*, weight factor.

[d] *SEE*, standard error of estimate.

[e] R^2, coefficient of determination.

[f] N_{imp}, weight factor for isolated $S = 1$ diradical.

Table 3.

B3LYP-computed values of intrachain J'/k for 2.[a]

	Dimer		Trimer	
	I (AB)	**II (BA)**	**ABA**	**BAB**
J'/k, 6–31G(d) [K]	−14.1	−12.7	−7.2	−12.0
J'/k, 6–311++G(d,p) [K]	−19.8	−9.2	-	-

[a]Broken symmetry triplets and quintets for dimers and trimers are used, respectively. Further details may be found in the SI (Table S8).